

Electro-weak Capture Reactions for Astrophysics

R. Schiavilla ^a

^aJefferson Lab, Newport News, Virginia 23606

and

Department of Physics, Old Dominion University, Norfolk, Virginia 23529

The status of *ab initio* microscopic calculations of the ${}^2\text{H}(p, \gamma){}^3\text{He}$ and ${}^3\text{He}(p, e^+\nu_e){}^4\text{He}$ reactions is reviewed. The methods used to generate accurate nuclear ground- and scattering-state wave functions, and to construct realistic electro-weak transition operators are described. The uncertainties in the theoretical predictions, particularly those relevant to the p ${}^3\text{He}$ weak capture, are discussed. For the dp radiative capture, the theoretical results are compared with the TUNL data in the energy range 0–100 keV.

1. Introduction

In the present talk I will review the progress made in the last couple of years in *ab initio* microscopic calculations of the ${}^2\text{H}(p, \gamma){}^3\text{He}$ [1] and ${}^3\text{He}(p, e^+\nu_e){}^4\text{He}$ [2] capture reactions. These reactions provide a sensitive testing ground for models of nuclear interactions and currents.

The outline of the talk is as follows. I will first describe the correlated-hyperspherical-harmonics method used to obtain accurate wave functions for the $A=3$ and 4 bound and scattering states. Next, I will discuss the model for the nuclear electromagnetic current, and will review our current understanding of the radiative capture reaction ${}^2\text{H}(p, \gamma){}^3\text{He}$. In the third part, I will discuss the model for the nuclear weak current, and present results for the proton weak capture on ${}^3\text{He}$. This process has lately received considerable attention, due to the Super-Kamiokande collaboration measurements of the energy spectrum of electrons recoiling from scattering with solar neutrinos [3].

The theoretical description of few-nucleon capture reactions constitutes a challenging problem from the standpoint of nuclear few-body theory. For example, since the $A=3$ and 4 bound states are approximate eigenstates of the magnetic moment operator, the corresponding transition matrix elements between these and the initial dp (or dn) and n ${}^3\text{He}$ states, occurring in the radiative captures, vanish due to orthogonality. As a result, these capture processes are extremely sensitive to: (i) small components in the wave functions, particularly the D-state admixtures generated by tensor interactions, (ii) many-body terms in the electro-weak current operator, and (iii) P-wave capture contributions.

2. Wave Functions

The nuclear Hamiltonian used in the calculations reported here has the form

$$H = \sum_i \frac{\mathbf{p}_i^2}{2m} + \sum_{i<j} v_{ij} + \sum_{i<j<k} V_{ijk} , \quad (1)$$

where the two-nucleon interaction is the Argonne v_{18} (AV18) model [4], and the three-nucleon interaction is the Urbana-IX (UIX) model [5]. This Hamiltonian predicts reasonably well the low-lying energy spectra of systems with $A \leq 8$ nucleons in “exact” Green’s function Monte Carlo calculations [6]. The experimental binding energies of the trineutrons and α particle are exactly reproduced, while those of the $A=6-8$ systems are underpredicted by a few percent. This underbinding becomes (relatively) more and more severe as the neutron-proton asymmetry increases. An additional failure of the AV18/UIX model is the underprediction of spin-orbit splittings in the excitation spectra of these light systems. These failures have in fact led to the development of new three-nucleon interaction models. These developments as well as a discussion of a number of issues regarding two-nucleon interactions, such as non-localities, unitary equivalence, etc., can be found in Friar’s [7] and Pandharipande’s [8] contributions to these proceedings.

While the nuclear interaction models above are simple to write down, bound- and scattering-state solutions for light nuclei have proven to be rather difficult to obtain. Intense work in this area and the continuing increase in computational capabilities have led, by now, to the development of a number of methods, each with different strengths and domains of applicability (for a review and an assessment of them, see Ref. [9]). The Faddeev-Yakubovsky and quantum Monte Carlo methods are reviewed, respectively, by Glöckle [10] and Pandharipande [8] in these proceedings. Here, I will briefly discuss the correlated-hyperspherical-harmonics (CHH) technique, as implemented by the Pisa group for the $A=3$ [11] and $A=4$ [12] nuclei, and summarize a number of results obtained for the bound-state properties and low-energy scattering parameters.

In essence, the CHH method consists in expanding the wave functions on a suitable basis, and in determining the expansion coefficients variationally. As an example, the trinucleon bound-state wave function is written as

$$\Psi = \sum_{\alpha} \frac{u_{\alpha}(\rho)}{\rho^{5/2}} \sum_{\text{cyclic } ijk} Z_{\alpha}(i; jk) , \quad (2)$$

where the hyperradius $\rho = \sqrt{x_i^2 + y_i^2}$ (\mathbf{x}_i and \mathbf{y}_i are the Jacobi variables), and the known functions $Z_{\alpha}(i; jk)$ are antisymmetric under the exchange $j \rightleftharpoons k$ and account for the angle ($\hat{\mathbf{x}}_i$ and $\hat{\mathbf{y}}_i$), spin (s_i and s_{jk}), isospin (t_i and t_{jk}), and hyperangle ($\phi_i = \cos^{-1}x_i/\rho$) dependence of channel α . Correlation factors, which account for the strong state-dependent correlations induced by the nucleon-nucleon interaction, are included in the functions $Z_{\alpha}(i; jk)$. The Rayleigh-Ritz variational principle, $\langle \delta_u \Psi | H - E_0 | \Psi \rangle = 0$, is used to determine the ground-state energy E_0 and the functions $u_{\alpha}(\rho)$. Carrying out the variations with respect to the u_{α} ’s leads to a set of coupled second-order differential equations, which are then solved by standard numerical techniques.

The Nd cluster wave function Ψ^{LSJJ_z} (again, as an example), having incoming orbital angular momentum L and channel spin S coupled to total JJ_z , is expressed as

$$\Psi^{LSJJ_z} = \Psi_C^{JJ_z} + \Psi_A^{LSJJ_z}, \quad (3)$$

where the term Ψ_C vanishes in the limit of large intercluster separation, and hence describes the system in the region where the particles are close to each other and their mutual interactions are large. The term $\Psi_A^{LSJJ_z}$, instead, describes the system in the asymptotic region, and contains the dependence upon the R -matrix elements, from which phase-shifts and mixing angles are obtained. The “core” wave function Ψ_C is expanded in the same basis as the bound-state wave function Ψ , and both the R -matrix elements and functions $u_\alpha(\rho)$ occurring in the expansion of Ψ_C are determined by making use of the Kohn variational principle. Results for the ${}^3\text{He}$ and ${}^4\text{He}$ binding energies, and p ${}^3\text{He}$ scattering lengths, obtained with the CHH method, are listed in Table 1.

Table 1

Binding energies, B_3 and B_4 , of ${}^3\text{He}$ and ${}^4\text{He}$, and p ${}^3\text{He}$ singlet and triplet S-wave scattering lengths, a_s and a_t , calculated with the CHH method using the AV18 and AV18/UIX Hamiltonian models.

Model	$B_3(\text{MeV})$	$B_4(\text{MeV})$	$a_s(\text{fm})$	$a_t(\text{fm})$
AV18	6.93	24.01	12.9	10.0
AV18/UIX	7.74	27.89	11.5	9.13
EXP	7.72	28.3	10.8 ± 2.6 [13]	8.1 ± 0.5 [13] 10.2 ± 1.5 [14]

3. The Nuclear Electromagnetic Current

The nuclear current operator consists of one- and many-body terms that operate on the nucleon degrees of freedom:

$$\mathbf{j}(\mathbf{q}) = \sum_i \mathbf{j}_i^{(1)}(\mathbf{q}) + \sum_{i<j} \mathbf{j}_{ij}^{(2)}(\mathbf{q}) + \sum_{i<j<k} \mathbf{j}_{ijk}^{(3)}(\mathbf{q}), \quad (4)$$

where \mathbf{q} is the momentum transfer, and the one-body operator $\mathbf{j}_i^{(1)}$ has the standard expression in terms of single-nucleon convection and magnetization currents. The two-body current operator has “model-independent” and “model-dependent” components (for a review, see Ref. [9]). The model-independent terms are obtained from the charge-independent part of the AV18, and by construction satisfy current conservation with this interaction. The leading operator is the isovector “ π -like” current obtained from the isospin-dependent spin-spin and tensor interactions. The latter also generate an isovector “ ρ -like” current, while additional model-independent isoscalar and isovector currents arise from the central and momentum-dependent interactions. These currents are short-ranged and numerically far less important than the π -like current. Finally, models for three-body

currents have been derived in Ref. [15], however the associated contributions have been found to be very small in studies of the magnetic structure of the trinucleons [15].

The model-dependent currents are purely transverse and therefore cannot be directly linked to the underlying two-nucleon interaction. Among them, those associated with the Δ -isobar are the most important ones in the momentum-transfer regime being discussed here. These currents are treated within the transition-correlation-operator (TCO) scheme [15,16], a scaled-down approach to a full $N+\Delta$ coupled-channel treatment. In the TCO scheme, the Δ degrees of freedom are explicitly included in the nuclear wave functions by writing

$$\Psi_{N+\Delta} = \left[\mathcal{S} \prod_{i<j} (1 + U_{ij}^{TR}) \right] \Psi, \quad (5)$$

where Ψ is the purely nucleonic component, \mathcal{S} is the symmetrizer and the transition correlations U_{ij}^{TR} are short-range operators, that convert NN pairs into $N\Delta$ and $\Delta\Delta$ pairs. In the results reported here, the Ψ is taken from CHH solutions of the AV18/UIX Hamiltonian with nucleons only interactions, while the U_{ij}^{TR} is obtained from two-body bound and low-energy scattering state solutions of the full $N-\Delta$ coupled-channel problem. Both $\gamma N\Delta$ and $\gamma\Delta\Delta$ M_1 couplings are considered with their values, $\mu_{\gamma N\Delta} = 3$ n.m. and $\mu_{\gamma\Delta\Delta} = 4.35$ n.m., obtained from data [16].

4. The pd Radiative Capture

There are now available many high-quality data, including differential cross sections, vector and tensor analyzing powers, and photon polarization coefficients, on the pd radiative capture at c.m. energies ranging from 0 to 2 MeV [17–20]. These data indicate that the reaction proceeds predominantly through S- and P-wave capture. The aim here is to verify the extent to which they can be described satisfactorily by a calculation based on a realistic Hamiltonian (the AV18/UIX model) and a current operator constructed consistently with the two- and three-nucleon interactions [1].

The calculated S -factor in the c.m. energy range 0–2 MeV is compared with data in Fig. 1, while the predicted angular distributions of the differential cross section $\sigma(\theta)$, vector and tensor analyzing powers $A_y(\theta)$ and $T_{20}(\theta)$, and photon linear polarization coefficient $P_\gamma(\theta)$ are compared with the TUNL data below 50 keV from Refs. [17,19] in Fig 2. The agreement between the full theory, including many-body current contributions, and experiment is generally good. However, a closer inspection of the figures reveals the presence of significant discrepancies between theory and experiment in the S -factor below 40 keV, and in the small angle behavior of $\sigma(\theta)$ and $T_{20}(\theta)$.

The S-wave capture proceeds mostly through the M_1 transitions connecting the doublet and quartet pd states to ${}^3\text{He}$ —the associated reduced matrix elements (RMEs) are denoted by m_2 and m_4 , respectively. The situation for P-wave capture is more complex, although at energies below 50 keV it is dominated by the E_1 transitions from the doublet and quartet pd states having channel spin $S=1/2$, whose RMEs we denote as p_2 and p_4 . The E_1 transitions involving the channel spin $S = 3/2$ states, while smaller, do play an important role in $T_{20}(\theta)$.

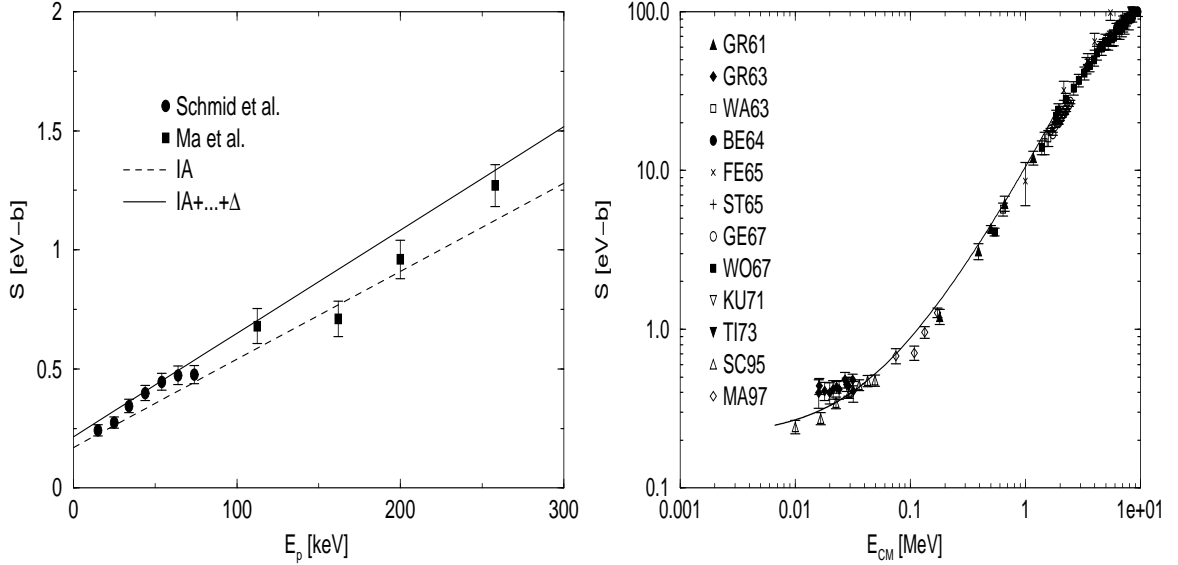


Figure 1. The S -factor for the ${}^2\text{H}(p,\gamma){}^3\text{He}$ reaction in the c.m. energy range 0–2 MeV, obtained with the AV18/UIX Hamiltonian model and one-body only (dashed line) or both one- and many-body (solid line) currents. In the right panel, only the results of the full calculation are shown.

The TUNL [19] and Wisconsin [20] groups have determined the leading M_1 and E_1 RMEs via fits to the measured observables. The results of this fitting procedure are compared with the calculated RMEs in Table 2. The phase of each RME is simply related to the elastic pd phase shift [20], which at these low energies is essentially the Coulomb phase shift. As can be seen from Table 2, the most significant differences between theoretical and experimental RMEs are found for $|p_4|$. The theoretical overprediction of p_4 is the cause of the discrepancies mentioned above in the low-energy (≤ 50 keV) S -factor and small angle $\sigma(\theta)$.

It is interesting to analyze the ratio $r_{E_1} \equiv |p_4/p_2|^2$. Theory gives $r_{E_1} \simeq 1$, while from the fit it results that $r_{E_1} \approx 0.74 \pm 0.04$. It is important to stress that the calculation of these RMEs is not influenced by uncertainties in the two-body currents, since their values are entirely given by the long-wavelength form of the E_1 operator (Siegert’s theorem), which has no spin-dependence (for a thorough discussion of the validity of the long-wavelength approximation in E_1 transitions, particularly suppressed ones, see Ref. [1]). It is therefore of interest to examine more closely the origin of the above discrepancy. If the interactions between the p and d clusters are switched off, the relation $r_{E_1} \simeq 1$ then simply follows from angular momentum algebra. Deviations of this ratio from one are therefore to be ascribed to differences induced by the interactions in the $S=1/2$ doublet and quartet wave functions. The AV18/UIX interactions in these channels do not change the ratio above significantly. It should be emphasized that the studies carried out up until now ignore, in the continuum states, the effects arising from electromagnetic interactions beyond the static Coulomb interaction between protons. It is not clear whether the

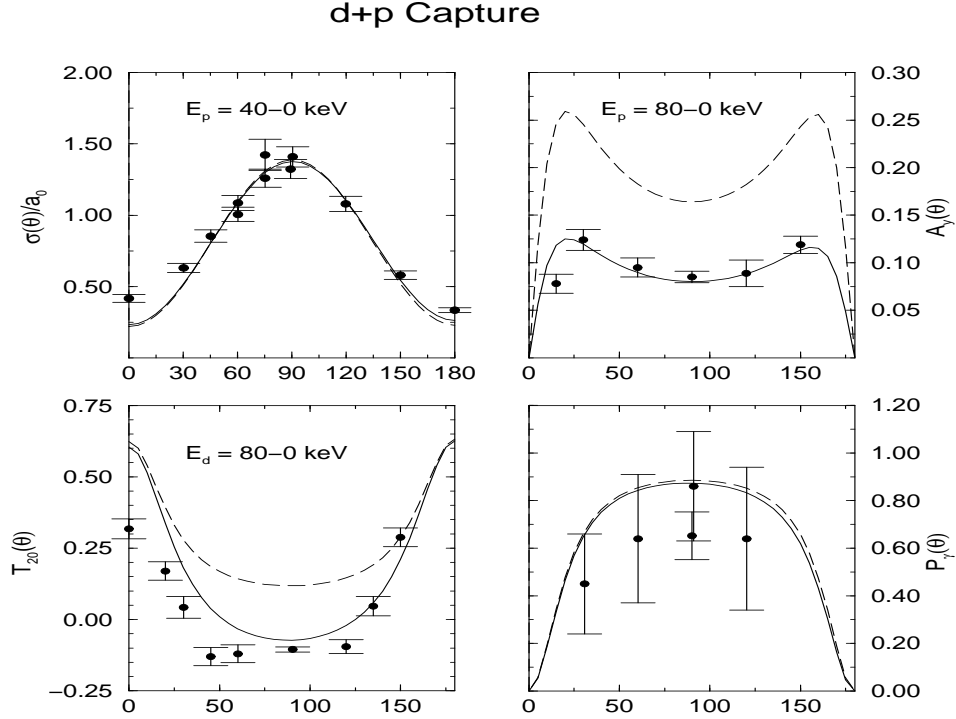


Figure 2. The energy integrated cross section $\sigma(\theta)/a_0$ ($4\pi a_0$ is the total cross section), vector analyzing power $A_y(\theta)$, tensor analyzing power $T_{20}(\theta)$ and photon linear polarization coefficient $P_\gamma(\theta)$ obtained with the AV18/UIX Hamiltonian model and one-body only (dashed line) or both one- and many-body (solid line) currents are compared with the experimental results of Ref. [17].

inclusion of these long-range interactions, in particular their spin-orbit component, could explain the splitting between the p_2 and p_4 RMEs observed at very low energy. Note that this discrepancy seems to disappear at 2 MeV [1].

Table 2

Magnitudes of the leading M_1 and E_1 RMEs for pd capture at $E_p = 40$ keV.

RME	IA	FULL	FIT
$ m_2 $	0.172	0.322	0.340 ± 0.010
$ m_4 $	0.174	0.157	0.157 ± 0.007
$ p_2 $	0.346	0.371	0.363 ± 0.014
$ p_4 $	0.343	0.378	0.312 ± 0.009

Finally, the doublet m_2 RME is underpredicted by theory at the 5 % level. On the other hand, the cross section for nd capture at thermal neutron energy is calculated to be $578 \mu\text{b}$ with the AV18/UIX model, which is 15 % larger than the experimental value (508 ± 15) μb [21]. Of course, M_1 transitions, particularly doublet ones, are significantly influenced by many-body current contributions. Indeed, an analysis of the isoscalar (μ_S)

and isovector (μ_V) magnetic moments of the trinucleons [15] suggests that the present model for the isoscalar two-body currents, constructed from the AV18 spin-orbit and quadratic-momentum dependent interactions, tends to overestimate μ_S by about 5 %. The experimental value for μ_V , however, is almost perfectly reproduced. The present model for two-body isoscalar currents needs to be improved.

5. The Nuclear Weak Current

The nuclear weak current and charge operators consist of vector and axial-vector parts, with corresponding one- and many-body components. The weak vector current and charge are constructed from the corresponding (isovector) electromagnetic terms, in accordance with the conserved-vector-current hypothesis, and thus have [2] “model-independent” and “model-dependent” components. The former are determined by the interactions, the latter include the transverse currents associated with Δ excitation.

The leading many-body terms in the axial current, in contrast to the case of the weak vector (or electromagnetic) current, are those due to Δ excitation, which are treated within the TCO scheme, discussed above. The axial charge operator includes the long-range pion-exchange term [22], required by low-energy theorems and the partially-conserved-axial-current relation, as well as the (expected) leading short-range terms constructed from the central and spin-orbit components of the nucleon-nucleon interaction, following a prescription due to Riska and collaborators [23].

The largest model dependence is in the weak axial current. The $N\Delta$ axial coupling constant g_A^* is not well known. In the quark-model, it is related to the axial coupling constant of the nucleon by the relations $g_A^* = (6\sqrt{2}/5)g_A$. This value has often been used in the literature in the calculation of Δ -induced axial current contributions to weak transitions. However, given the uncertainties inherent to quark-model predictions, a more reliable estimate for g_A^* is obtained by determining its value phenomenologically. It is well established by now [24] that one-body axial current lead to a $\simeq 4\%$ underprediction of the measured Gamow-Teller matrix element in tritium β -decay. This small 4 % discrepancy can then be used to determine g_A^* [2]. While this procedure is inherently model dependent, its actual model dependence is in fact very weak, as has been shown in Ref. [24].

6. The $p^3\text{He}$ Weak Capture

The hep capture process is induced by the weak interaction Hamiltonian H_W . After partial-wave expansion of the $p^3\text{He}$ scattering state, the transition amplitude is written as [2]

$$\langle {}^4\text{He} | H_W | p^3\text{He}; s_1, s_3 \rangle = G_V \sum_{LSJJ_z} C_{s_1 s_3 J_z}^{LSJ} \langle \Psi_4 | l^\sigma j_\sigma^\dagger(\mathbf{q}) | \Psi_{1+3}^{LSJJ_z} \rangle, \quad (6)$$

where l^σ and $j_\sigma(\mathbf{q})$ are the lepton and nuclear weak currents, respectively, and $C_{s_1 s_3 J_z}^{LSJ}$ denotes products of Clebsch-Gordan coefficients. The study reported in Ref. [2] includes all transitions connecting the $p^3\text{He}$ S- and P-wave channels to the ${}^4\text{He}$ bound state. The corresponding wave functions are obtained from realistic Hamiltonians consisting of the AV18/UIX and older AV14/UVIII [25] interaction models.

The calculated values for the astrophysical S -factor in the energy range 0–10 keV are listed in Table 3. Inspection of the table shows that: (i) the energy dependence is rather weak, the value at 10 keV is only about 4 % larger than that at 0 keV; (ii) the P-wave capture states are found to be important, contributing about 40 % of the calculated S -factor. However, the contributions from D-wave channels are expected to be very small, as explicitly verified in ${}^3\text{D}_1$ capture. (iii) The many-body axial currents associated with Δ excitation play a crucial role in the (dominant) ${}^3\text{S}_1$ capture, where they reduce the S -factor by more than a factor of four; thus the destructive interference between the one- and many-body current contributions, obtained in Ref. [16], is confirmed in the study of Ref. [2], based on more accurate wave functions. The (suppressed) one-body contribution comes mostly from transitions involving the D-state components of the ${}^3\text{He}$ and ${}^4\text{He}$ wave functions, while the many-body contributions are predominantly due to transitions connecting the S-state in ${}^3\text{He}$ to the D-state in ${}^4\text{He}$, or viceversa.

Table 3

The *hep* S -factor, in units of 10^{-20} keV b, calculated with CHH wave functions corresponding to the AV18/UIX Hamiltonian model, at p ${}^3\text{He}$ c.m. energies $E=0, 5, \text{ and } 10$ keV. The rows labelled “one-body” and “full” list the contributions obtained by retaining the one-body only and both one- and many-body terms in the nuclear weak current. The contributions due the ${}^3\text{S}_1$ channel only and all S- and P-wave channels are listed separately.

	$E=0$ keV		$E=5$ keV		$E=10$ keV	
	${}^3\text{S}_1$	S+P	${}^3\text{S}_1$	S+P	${}^3\text{S}_1$	S+P
one-body	26.4	29.0	25.9	28.7	26.2	29.3
full	6.38	9.64	6.20	9.70	6.36	10.1

The chief conclusion of Ref. [2] is that the *hep* S -factor is predicted to be $\simeq 4.5$ times larger than the value adopted in the standard solar model (SSM) [26]. This enhancement, while very significant, is smaller than that first suggested in Ref. [27]. Even though this result is inherently model dependent, it is unlikely that the model dependence is large enough to accommodate a drastic increase in the value obtained here. Indeed, calculations using Hamiltonians based on the AV18 two-nucleon interaction only and the older AV14/UVIII two- and three-nucleon interactions predict zero energy S -factor values of 12.1×10^{-20} keV b and 10.2×10^{-20} keV b, respectively. It should be stressed, however, that the AV18 model, in contrast to the AV14/UVIII, does not reproduce the experimental binding energies and low-energy scattering parameters of the three- and four-nucleon systems. The AV14/UVIII prediction is only 6 % larger than the AV18/UIX zero-energy result. This 6 % variation should provide a fairly realistic estimate of the theoretical uncertainty due to the model dependence.

The implications of these predictions for the SuperKamiokande (SK) solar neutrino spectrum are summarized Fig. 3. The SK results are presented as the ratio of the measured electron spectrum to that expected in the SSM with no neutrino oscillations. Over most of the spectrum, this ratio is constant at $\simeq 0.5$. At the highest energies, however, an excess

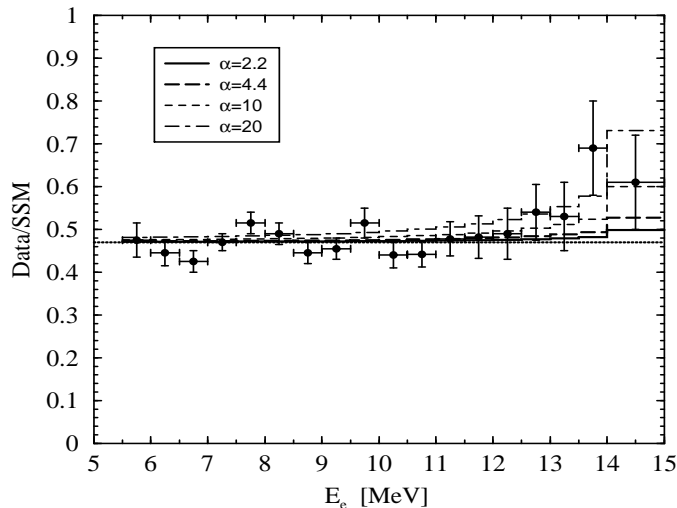


Figure 3. Electron energy spectrum for the ratio between the Super-Kamiokande 825-days data and the expectation based on unoscillated ${}^8\text{B}$ neutrinos [26]. See text for an explanation of the symbols.

relative to $0.5 \times \text{SSM}$ is seen (though it has diminished in successive data sets). The SK 825-day data are shown by the points in Fig. 3 (the error bars denote the combined statistical and systematic error). In the figure, the ratio of the *hep* flux to its value in the SSM (based on the *hep* S-factor prediction of Ref. [16]) is denoted by α , defined as $\alpha \equiv (S_{\text{new}}/S_{\text{SSM}}) \times P_{\text{osc}}$, where P_{osc} is the *hep*-neutrino suppression constant. Presently, $\alpha = (10.1 \times 10^{-20} \text{ keV b}) / (2.3 \times 10^{-20} \text{ keV b}) = 4.4$, if *hep* neutrino oscillations are ignored. The lines in Fig. 3 indicate the effect of various values of α on the ratio of the electron spectrum with both ${}^8\text{B}$ and *hep* to that with only ${}^8\text{B}$ (the SSM). In calculating this ratio, the ${}^8\text{B}$ flux in the numerator has been suppressed by 0.47, the best-fit constant value for the observed suppression. If the *hep* neutrinos are suppressed by $\simeq 0.5$, then $\alpha = 2.2$. Two other arbitrary values of α (10 and 20) are shown for comparison. It appears that the prediction of Ref. [2] is unable to explain the distortion observed in the spectrum at the highest energies.

7. Outlook

Improvements in the modeling of two- and three-nucleon interactions and nuclear electro-weak currents, and the significant progress made in the last few years in the description of bound and continuum wave functions, make it now possible to perform first-principle calculations of interesting low-energy reactions involving light nuclei. While the extension of the CHH technique to treat systems with $A \geq 6$ may prove difficult, variational and Green's function Monte Carlo methods should be able to deal with them effectively, in particular their pre-capture continuum states. Experimentally known electromagnetic and weak transitions of systems in the mass range $4 \leq A \leq 9$ will provide powerful constraints on models of nuclear currents. Work along these lines is being vig-

orously pursued.

8. Acknowledgments

I wish to thank L.E. Marcucci, M. Viviani, A. Kievsky, and S. Rosati for their many important contributions to the work reported here. I also like to gratefully acknowledge the support of the U.S. Department of Energy under contract number DE-AC05-84ER40150.

REFERENCES

1. M. Viviani, A. Kievsky, L.E. Marcucci, S. Rosati, and R. Schiavilla, Phys. Rev. C **61**, 064001 (2000).
2. L.E. Marcucci, R. Schiavilla, M. Viviani, A. Kievsky, and S. Rosati, nucl-th/0003065, Phys. Rev. Lett. in press; L.E. Marcucci, R. Schiavilla, M. Viviani, A. Kievsky, S. Rosati, and J.F. Beacom, nucl-th/0006005, submitted to Phys. Rev. C.
3. Y. Fukuda *et al.*, Phys. Rev. Lett. **82**, 2430 (1999); M.B. Smy, hep-ex/9903034.
4. R.B. Wiringa, V.G.J. Stoks, and R. Schiavilla, Phys. Rev. C **51**, 38 (1995).
5. B.S. Pudliner, V.R. Pandharipande, J. Carlson, and R.B. Wiringa, Phys. Rev. Lett. **74**, 4396 (1995).
6. R.B. Wiringa, S.C. Pieper, J. Carlson, and V.R. Pandharipande, Phys. Rev. C **62**, 014001 (2000).
7. J.L. Friar, these proceedings.
8. V.R. Pandharipande, these proceedings.
9. J. Carlson and R. Schiavilla, Rev. Mod. Phys. **70**, 743 (1998).
10. W. Glöckle, these proceedings.
11. A. Kievsky, M. Viviani, and S. Rosati, Nucl. Phys. **A551**, 241 (1993); Nucl. Phys. **A577**, 511 (1994); A. Kievsky *et al.*, Phys. Rev. C **58**, 3085 (1998).
12. M. Viviani, A. Kievsky, and S. Rosati, Few-Body Syst. **18**, 25 (1995); M. Viviani, S. Rosati, and A. Kievsky, Phys. Rev. Lett. **81**, 1580 (1998).
13. M.T. Alley and L.D. Knutson, Phys. Rev. C **48**, 1901 (1993).
14. P.E. Tegnér and C. Bargholtz, Astrophys. J. **272**, 311 (1983).
15. L.E. Marcucci, D.O. Riska, and R. Schiavilla, Phys. Rev. C **58**, 3069 (1998).
16. R. Schiavilla, R.B. Wiringa, V.R. Pandharipande, and J. Carlson, Phys. Rev. C **45**, 2628 (1992).
17. G.J. Schmid *et al.*, Phys. Rev. Lett. **76**, 3088 (1996).
18. L. Ma *et al.*, Phys. Rev. C **55**, 588 (1997).
19. E.A. Wulf *et al.*, Phys. Rev. C **61**, 021601(R) (1999).
20. M.K. Smith and L.D. Knutson, Phys. Rev. Lett. **82**, 4591 (1999).
21. E.T. Journey, P.J. Bendt, and J.C. Browne, Phys. Rev. C **25**, 2810 (1982).
22. K. Kubodera, J. Delorme, and M. Rho, Phys. Rev. Lett. **40**, 755 (1978).
23. M. Kirchbach, D.O. Riska, and K. Tsushima, Nucl. Phys. **A542**, 616 (1992).
24. R. Schiavilla *et al.*, Phys. Rev. C **58**, 1263 (1998).
25. R.B. Wiringa, R.A. Smith, and T.L. Ainsworth, Phys. Rev. C **29**, 1207 (1984); R.B. Wiringa, Phys. Rev. C **43**, 1585 (1991).
26. J.N. Bahcall, S. Basu, and M.H. Pinsonneault, Phys. Lett. B **433**, 1 (1998).
27. J.N. Bahcall and P.I. Krastev, Phys. Lett. B **436**, 243 (1998).